Capturing Out-of-Plane Shear Failures in the Analysis of Reinforced Concrete Shells

Trevor D. Hrynyk[1] and Frank J. Vecchio, M.ASCE[2]

Abstract: A procedure for nonlinear analysis of RC slabs and shell structures is presented. Cracked RC is treated as an orthotropic material governed by a smeared rotating crack procedure and the constitutive formulations of the disturbed stress field model. The analysis procedure is implemented within the framework of a finite-element program employing layered thick-shell elements that consider out-of-plane (through-thickness) shear deformations. A simple modification method employing an effective shear strain concept is introduced to improve the out-of-plane performance of the layered shell element for RC applications. The adequacy of the procedure is verified using test data of RC members controlled by out-of-plane shear failure mechanisms and elements under combined in-plane and out-of-plane loading scenarios. The nonlinear finite-element program is shown to be suitable for elements exhibiting ductile or brittle responses, and the shear modification method introduced is found to be capable of capturing out-of-plane shear failures. **DOI: 10.1061/(ASCE)ST.1943-541X.0001311.** © *2015 American Society of Civil Engineers.*

Author keywords: Reinforced concrete; Shear; Out-of-plane shear; Thick shell; Slabs; Nonlinear analysis; Finite element; Analysis and computation.

Introduction

RC shells are employed frequently in the design of modern concrete infrastructure because their outstanding load-carrying capabilities make them ideal candidates for demanding structural applications. Today, computer-based analytical procedures are commonly used in the design of RC structures. In the specific case of RC shells that are often characterized by curvilinear geometries and are subjected to complex loading conditions, the use of computational modeling procedures is particularly appealing because they can provide a practical approach toward the design and assessment of such structures.

The introduction of multilayered shell analysis procedures represents a significant advancement toward the current state of the art in RC shell modeling. By subdividing a shell element into a series of layers, each with uniform in-plane stress and strain conditions, stiffness variations through the thickness are represented discretely. Compatibility assumptions used to describe the in-plane strain variation through the thickness, e.g., plane sections remain plane, provide a computational procedure similar to that employed for two-dimensional membranes that is capable of analyzing elements under coexisting bending moments and in-plane membrane forces. Hand et al. (1973) and Lin and Scordelis (1975) reported early applications of layered shell elements for RC applications. In the late 1970s, Schnobrich (1977) provided a general review of RC finite-element modeling techniques that were available at that time. It was suggested that for plate and shell structures dominated by combined flexure and membrane forces, the types of elements employed by Hand et al. (1973) and Lin and Scordelis (1975) were the most suitable of those available. However, Schnobrich noted that if out-of-plane shear was relevant, alternative three-dimensional models should be employed.

In the design of RC shell structures subjected to combined bending moments, membrane forces, and out-of-plane shear forces, shell-type analysis procedures are commonly used to evaluate the structure response under coexisting membrane forces and bending moments, and supplemental analyses are used to investigate out-of-plane shear resistance. The validity of this approach is somewhat unfounded because most of the supplemental procedures used to compute out-of-plane shear strength are empirical and were developed for much simpler beam-type RC elements (Adebar 1989; Collins and Mitchell 1997). Thus, significant research efforts have been focused toward the development of RC shell analysis procedures that can adequately consider conditions of combined membrane forces, bending moments, and out-of-plane shear forces.

Owen and Figueiras (1984) were among the early investigators to report RC shell finite-element analysis procedures that considered out-of-plane shear forces. The authors employed a layered thick-shell finite element developed on the basis of the Mindlin theory (Mindlin 1951), inherently assuming that out-of-plane shear strains are constant through the thickness of the element. Polak and Vecchio (1993) later modified the thick-shell finite-element program developed by Owen and Figueiras (1984), such that the behavior of cracked RC was modeled in accordance with the formulations of the modified compression field theory (Vecchio and Collins 1986). Similar thick-shell finite-element procedures developed on the basis of the Mindlin theory that employed different RC behavioral models have also been reported (Song et al. 2002; Maekawa et al. 2003).

Others have developed layered sectional analysis tools that can be used to investigate the behavior of a single RC shell element under user-defined loading. Examples can be found in the work of Kirschner and Collins (1986), Adebar and Collins (1991), and Bentz (2000). In comparison to finite-element procedures, sectional analysis tools are generally less restrictive in their development and, as a result, often employ rigorous solution methods to model

[1]Assistant Professor, Dept. of Civil, Architectural, and Environmental Engineering, Univ. of Texas at Austin, Austin, TX 78712 (corresponding author). E-mail: thrynyk@utexas.edu

[2]Professor, Dept. of Civil Engineering, Univ. of Toronto, Toronto, ON, Canada M5S 1A4.

Note. This manuscript was submitted on January 14, 2014; approved on February 21, 2015; published online on April 7, 2015. Discussion period open until September 7, 2015; separate discussions must be submitted for individual papers. This paper is part of the ***Journal of Structural Engineering***, © ASCE, ISSN 0733-9445/04015058(11)/$25.00.

out-of-plane shear behavior. However, their application is limited by the requirement of the user to predetermine critical structural elements and specify appropriate loading conditions.

The nonlinear analysis procedure presented in this paper is developed on the basis of the thick-shell finite-element program reported by Owen and Figueiras (1984) and subsequent work presented by Polak and Vecchio (1993). The introduction of a simple modification procedure is used to improve the performance of the Mindlin-type finite elements for the analysis of RC under out-of-plane shear loading conditions. Combined with the formulations of the disturbed stress field model to represent the behavior of cracked RC, the modified solution algorithm is found to accurately capture the response of RC slabs and shell structures under combined in-plane and out-of-plane loading scenarios and, in contrast to much of the related work presented in the literature, the procedure is verified using experimental data in which out-of-plane shear failure mechanisms govern. The resulting finite-element program can be used to efficiently model RC subassemblies or, in some cases, full RC shell structures while still adequately capturing RC material response and failure mechanisms.

Finite-Element Overview

The presented nonlinear analysis procedure is implemented within the framework of an isoparametric thick-shell finite-element analysis program. Detailed presentation of the finite-element formulation is available elsewhere (Figueiras and Owen 1984); however, the following section provides an overview of several key attributes of the shell element.

The quadratic heterosis shell element employed is developed using a combination of serendipity shape functions for translational degrees of freedom (DOFs) and Lagrangian shape functions for rotational DOFs. This approach, combined with a selective numerical integration scheme to avoid shear locking phenomena, results in an element that permits curved geometries and variable thicknesses, exhibits good performance in thick- and thin-shell applications, and avoids the development of spurious zero-energy modes arising from reduced integration procedures. A total of 42 DOFs are considered in the nine-noded shell. The eight nodes forming the edges of the element each have five DOFs (three translations and two rotations) and the ninth node located at the center of the element has two rotational DOFs.

Relevant to the work comprising this study, out-of-plane shear deformations are developed by way of a thick-shell formulation in accordance with Mindlin theory (Mindlin 1951). Mindlin-type finite elements are formulated on the basis of the assumptions that (1) plane sections before deformation remain plane after deformation, but not necessarily normal to the element midsurface, and (2) stresses normal to the midsurface, i.e., out-of-plane stresses, are negligible. Fig. 1 illustrates the element deformation assumptions and shows how the sectional rotation is assumed to be composed of two parts: bending deformations, $\delta w/\delta x$, and shear deformations, ϕ_x. For the section to remain planar under combined bending and shear, the out-of-plane shear strains are assumed to be constant through the thickness. The second assumption implies that deformations normal to the surface of the element are not considered in the element displacement field. The strain set that is computed from the nodal displacements (relative to the local x, y, z-system) for a given point within the element is

$$\{\varepsilon\} = \langle \varepsilon_x \quad \varepsilon_y \quad \gamma_{xy} \quad \gamma_{xz} \quad \gamma_{yz} \rangle \tag{1}$$

The out-of-plane normal strain, ε_z, which is absent from Eq. (1), is computed on the basis of the assumption that out-of-plane normal stresses are negligible and is dependent on the material stiffness and strain condition at the given point.

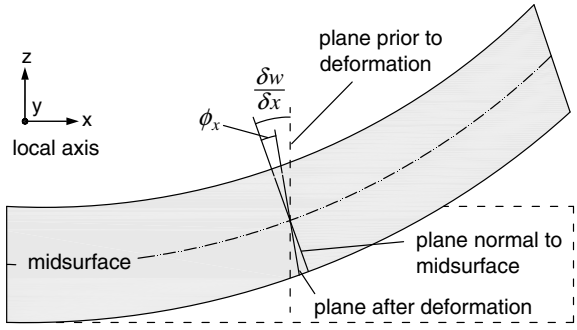

Fig. 1. Mindlin element deformation behavior

A layered approach is used to account for the nonlinear variation of material stress and stiffness through the thickness of the shell [Fig. 2(a)]. Local stresses are assumed to be constant over the layer height and are integrated using a trapezoidal rule. In-plane reinforcement layers can be defined in any planar orientation and are represented discretely within the thickness, i.e., in-plane reinforcement is not smeared within the concrete layers. If present, out-of-plane reinforcement (oriented in local z) is treated in a smeared manner as a property of the concrete layers. Integration of the concrete and steel layer stresses through the thickness of the element yields the sectional force resultants presented in Fig. 2(b).

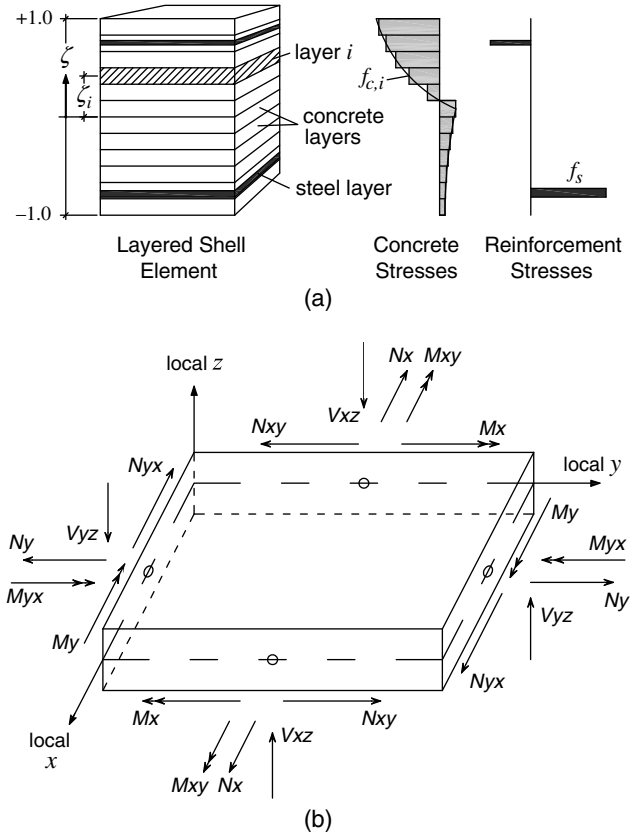

Fig. 2. Shell element attributes: (a) layered modeling approach; (b) sectional force resultants

RC Material Modeling

In the analysis procedure presented, cracked RC is modeled in accordance with the formulations of the disturbed stress field model (DSFM) (Vecchio 2000). Developed as an extension of the modified compression field theory (MCFT) (Vecchio and Collins 1986), the DSFM serves as a generalized approach for modeling the behavior of RC elements subjected to biaxial loading conditions. Central to the model is the treatment of cracked RC as an orthotropic material with its own set of governing constitutive equations. Formulated as a smeared hybrid rotating-fixed crack model, stresses and strains are treated in an average sense and are allowed to gradually reorient as a result of changing load and material response. The composite element, which consists of cracked concrete and in-plane reinforcement, is governed by equations of equilibrium, compatibility, and constitutive material models. Although cracks are considered smeared and stresses and strains are averaged, a key feature of the DSFM is the consideration of the local behavior at crack locations that accounts for the influence of localized stress conditions, variable or changing crack widths, and crack-slip deformations along crack surfaces. The inclusion of rigid body slip along the cracks in the element compatibility modeling of the DSFM is one of the primary differences from the formulations of the MCFT.

The DSFM and MCFT behavioral models have been heavily cited, referenced, and discussed throughout the database of RC literature and, as such, detailed formulations pertaining to the two models are not presented. However, minor procedural modifications required to apply the DSFM in the analysis of RC shell elements under three-dimensional loading conditions are summarized.

Local Conditions at the Crack

Examination of local behavior at crack locations is a key feature of the DSFM. Crack-slip deformations are assumed to stem directly from the development of shear stresses on the crack surface and are incorporated in an averaged sense in the governing compatibility relations.

Fig. 3 illustrates a cracked RC element that is subjected to three-dimensional stress conditions and contains one arbitrarily oriented reinforcement component, which is denoted as reinforcement component i. Examination of the principal planes illustrated in Fig. 3 and defined according to net concrete strains shows that in the case of cracking in the 1-direction, average concrete stresses f_{c2} and f_{c3}, both of which were assumed to be compressive in this sample case, have no influence on the local stresses at the crack location. To maintain equilibrium in the principal 1-direction, increased reinforcement stress across the crack, f_{sicr}, is required to balance the average concrete tensile stress f_{c1}, which is attributed to tension stiffening effects. In turn, shear stress on the crack surface balances the stress in the 2- and 3-directions resulting from the localized increase of reinforcement stress.

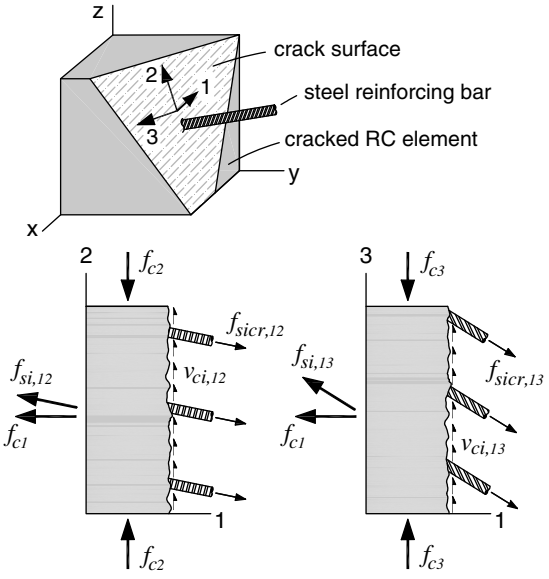

Fig. 3. Cracked RC element under three-dimensional stress conditions

To accommodate the three-dimensional nature of the local behavior at the crack locations, the magnitude of the resultant shear stress on the crack in the 1-direction $v_{ci,1}$ is calculated as the vector sum of the local shear stresses $v_{ci,12}$ and $v_{ci,13}$ presented in Fig. 3 [refer to Eq. (2)]. This resultant local shear stress is used in accordance with the relations of the DSFM to calculate slip deformations and average slip strains, which are considered in the element compatibility

$$v_{ci,1} = \sqrt{v_{ci,12}^2 + v_{ci,13}^2} \tag{2}$$

Compression Softening

In the original formulation of the DSFM, the compression softening parameter β_d for an element subjected to biaxial stress conditions is computed from (Vecchio 2000)

$$\beta_d = \frac{1}{1 + C_s C_d} \leq 1.0 \tag{3a}$$

$$C_d = 0.35(-\varepsilon_{c1}/\varepsilon_{c2} - 0.28)^{0.80} \tag{3b}$$

where ε_{c1} and ε_{c2} represent the net tensile and net compressive strains in the concrete, respectively; and C_s is a factor used to specify whether or not slip deformations are considered in the analysis. To account for the presence of three-dimensional stress conditions, C_d is computed from the following:

$$\text{If } \varepsilon_{c2} > 0\text{: } C_d = 0.35\left(-\sqrt{\varepsilon_{c1}^2 + \varepsilon_{c2}^2}/\varepsilon_{c3} - 0.28\right)^{0.80} \tag{4a}$$

$$\text{If } \varepsilon_{c2} \leq 0\text{: } C_d = 0.35(-\varepsilon_{c1}/\varepsilon_{c3} - 0.28)^{0.80} \tag{4b}$$

If the intermediate principal concrete strain ε_{c2} is compressive or zero, Eq. (4) is of the same form as that for an element under biaxial stress conditions. If ε_{c1} and ε_{c2} are both tensile, the compression softening factor is a function of an effective tensile strain, which is computed as the vector sum of the principal tensions. This approach has been used previously to analyze RC elements under three-dimensional loading conditions in accordance with the MCFT (Kirschner and Collins 1986; Adebar and Collins 1991; Polak and Vecchio 1993).

Finite-Element Implementation

Material Matrix Development

In the procedure developed, concrete and steel layers are analyzed individually and comprise unique contributions toward the stiffness matrix forming the shell element. Material matrices for concrete and steel are developed separately; however, their material

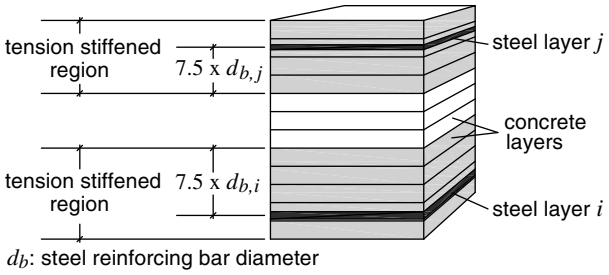

Fig. 4. Tension stiffening tributary regions

responses are somewhat interdependent. To evaluate concrete material behavior, steel reinforcement layers are smeared across the width of the element and through some portion of the element thickness. Normal to the plane, the tributary area pertaining to an individual steel component is assumed to extend a distance of 7.5 times the bar diameter from the reinforcement location, as suggested by CEB-FIP MC90 (Comité EURO-International du Béton 1990) (Fig. 4). Concrete layers that lie within this tributary reinforcement area are subject to tension-stiffening effects and require examination of the local behavior at crack locations. However, it is important to note that the reinforcing bars are not considered in a smeared sense when evaluating stiffness contributions from steel layers, but are treated discretely as additional layers comprising the RC shell element.

In the general case, the total strains, ε, acting within a concrete layer of the shell element are composed of (1) net strains, ε_c, (2) elastic offsets, ε_c^o, which may include thermal strains, shrinkage strains, expansions due to Poisson's effect and dilatation, (3) plastic offsets, ε_c^p, that represent permanent damage incurred under prior loading, and (4) crack-slip strains that result from shear slip on the crack surface, ε_c^s, which are inherent to relations of the DSFM. The total concrete strains can be expressed as

$$\begin{aligned}\{\varepsilon\} &= \{\varepsilon_c\} + \{\varepsilon_c^o\} + \{\varepsilon_c^p\} + \{\varepsilon_c^s\} \\ &= \langle\, \varepsilon_x \quad \varepsilon_y \quad \varepsilon_z \quad \gamma_{xy} \quad \gamma_{xz} \quad \gamma_{yz} \,\rangle\end{aligned} \tag{5}$$

Assuming that reinforcement and concrete possess perfect bond, the total strains developed in the ith steel layer are equal to the total strains in the concrete at common locations. The total reinforcement strains are composed of (1) net strains, $\varepsilon_{s,i}$, (2) elastic offsets, $\varepsilon_{s,i}^o$, which may include thermal strains and prestrains, and (3) plastic offsets, $\varepsilon_{s,i}^p$, that represent yielding or damage incurred under prior loading

$$\{\varepsilon\}_i = \{\varepsilon_s\}_i + \{\varepsilon_s^o\}_i + \{\varepsilon_s^p\}_i = \langle\, \varepsilon_x \quad \varepsilon_y \quad \varepsilon_z \quad \gamma_{xy} \quad \gamma_{xz} \quad \gamma_{yz} \,\rangle_i \tag{6}$$

Recall that the out-of-plane strain term ε_z is not calculated from the displacement field of the shell element but is computed on the basis of the zero out-of-plane stress assumption. The following subsection provides the calculation of ε_z.

Concrete principal strains ($\varepsilon_{c1}, \varepsilon_{c2}, \varepsilon_{c3}$) and their corresponding direction cosine vectors are calculated using the local net strains presented in Eq. (5). The concrete principal stresses (f_{c1}, f_{c2}, f_{c3}) are computed in accordance with the formulations of the DSFM. Secant moduli pertaining to the concrete material stiffness in the principal stress directions are calculated using

$$\bar{E}_{c1} = \frac{f_{c1}}{\varepsilon_{c1}}; \qquad \bar{E}_{c2} = \frac{f_{c2}}{\varepsilon_{c2}}; \qquad \bar{E}_{c3} = \frac{f_{c3}}{\varepsilon_{c3}} \tag{7}$$

The secant shear moduli are calculated according to

$$\begin{aligned}&\bar{G}_{c12} = \frac{\bar{E}_{c1} \cdot \bar{E}_{c2}}{\bar{E}_{c1} + \bar{E}_{c2}}; \qquad \bar{G}_{c13} = \frac{\bar{E}_{c1} \cdot \bar{E}_{c3}}{\bar{E}_{c1} + \bar{E}_{c3}}; \\ &\bar{G}_{c23} = \frac{\bar{E}_{c2} \cdot \bar{E}_{c3}}{\bar{E}_{c2} + \bar{E}_{c3}}\end{aligned} \tag{8}$$

The orthotropic concrete material matrix, $[D_c]'$, relative to the principal stress directions is assembled as

$$[D_c]' = \begin{bmatrix} \bar{E}_{c1} & 0 & 0 & 0 & 0 & 0 \\ 0 & \bar{E}_{c2} & 0 & 0 & 0 & 0 \\ 0 & 0 & \bar{E}_{c3} & 0 & 0 & 0 \\ 0 & 0 & 0 & \bar{G}_{c12} & 0 & 0 \\ 0 & 0 & 0 & 0 & \bar{G}_{c13} & 0 \\ 0 & 0 & 0 & 0 & 0 & \bar{G}_{c23} \end{bmatrix} \tag{9}$$

Recall that Poisson's effect is treated as an elastic offset and, as such, the material matrix presented in Eq. (9) will always be diagonal. Transformation to the local x, y, z-coordinate system is performed using an appropriate transformation matrix $[T_c]$ (Cook et al. 1989)

$$[D_c] = [T_c]^T [D_c]' [T_c] \tag{10}$$

Although the matrix presented in Eq. (9) will always be diagonal, the local material stiffness matrix presented in Eq. (10) can be fully populated, and, as such, there is a coupled effect between the in-plane and out-of-plane responses of the RC shell element.

Analogous to the approach used to evaluate the local concrete material matrix $[D_c]$, stiffness contributions from in-plane reinforcement layers are developed from their respective secant moduli and used to compute reinforcement material matrices. Assuming that the reinforcing bars do not carry shear stresses, i.e., dowel stresses, the contribution from the ith reinforcement layer is defined as

$$[D_s]_i' = \begin{bmatrix} \rho_{s,i} \cdot \bar{E}_{s,i} & 0 & 0 & 0 & 0 & 0 \\ 0 & 0 & 0 & 0 & 0 & 0 \\ 0 & 0 & 0 & 0 & 0 & 0 \\ 0 & 0 & 0 & 0 & 0 & 0 \\ 0 & 0 & 0 & 0 & 0 & 0 \\ 0 & 0 & 0 & 0 & 0 & 0 \end{bmatrix} \tag{11}$$

where $\rho_{s,i}$ = reinforcement ratio corresponding to the ith layer of reinforcement, and the corresponding secant modulus is computed from

$$\bar{E}_{s,i} = \frac{f_{s,i}}{\varepsilon_{s,i}} \tag{12}$$

The in-plane reinforcement stiffness matrix is transformed from the longitudinal axis of the reinforcing bar to the local x, y, z-coordinate system. The resulting local reinforcement stiffness matrix for the ith layer of reinforcement containing only in-plane stiffness contributions is

$$[D_s]_i = [T_s]^T [D_s]_i' [T_s] \tag{13}$$

If present, out-of-plane reinforcement is treated as a smeared property of the concrete layers. The composite material matrix

$[D_{cz}]$ represents the combined stiffness of the concrete and the out-of-plane reinforcement oriented in the local z-direction

$$[D_{cz}] = [D_c] + [D_z] \tag{14}$$

where $[D_z]$ = local material matrix for the out-of-plane reinforcement and is computed directly without transformation as

$$[D_z] = \begin{bmatrix} 0 & 0 & 0 & 0 & 0 & 0 \\ 0 & 0 & 0 & 0 & 0 & 0 \\ 0 & 0 & \rho_z \cdot \bar{E}_z & 0 & 0 & 0 \\ 0 & 0 & 0 & 0 & 0 & 0 \\ 0 & 0 & 0 & 0 & 0 & 0 \\ 0 & 0 & 0 & 0 & 0 & 0 \end{bmatrix} \tag{15}$$

where $\bar{E}_z$ is calculated in the same manner as the secant moduli for in-plane reinforcement contributions [Eq. (12)]; and ρ_z represents the out-of-plane reinforcement ratio.

The stresses in the concrete layers are calculated using the following equilibrium relation:

$$\{\sigma_{cz}\} = [D_{cz}]\{\varepsilon\} - \{\sigma^o_{cz}\} \tag{16}$$

To accommodate strain offsets, the pseudostress vector $\{\sigma^o_{cz}\}$ is required in the preceding equilibrium equation. The pseudostresses pertaining to the concrete layers are calculated as

$$\{\sigma^o_{cz}\} = \{\sigma^o_c\} + \{\sigma^o_z\} = \langle\, \sigma^o_{cz_x} \quad \sigma^o_{cz_y} \quad \sigma^o_{cz_z} \quad \tau^o_{cz_{xy}} \quad \tau^o_{cz_{xz}} \quad \tau^o_{cz_{yz}} \,\rangle \tag{17a}$$

$$\{\sigma^o_c\} = [D_c](\{\varepsilon^o_c\} + \{\varepsilon^p_c\} + \{\varepsilon^s_c\}) \tag{17b}$$

$$\{\sigma^o_z\} = [D_z](\{\varepsilon^o_z\} + \{\varepsilon^p_z\}) \tag{17c}$$

Similarly, steel layer stresses are calculated using Eq. (18*a*), and the steel layer pseudostress vector $\{\sigma^o_s\}$ is calculated from Eq. (18*b*)

$$\{\sigma_s\} = [D_s]\{\varepsilon\} - \{\sigma^o_s\} \tag{18a}$$

$$\{\sigma^o_s\} = [D_s](\{\varepsilon^o_s\} + \{\varepsilon^p_s\}) \tag{18b}$$

Enforcing Zero Normal Stress

To enforce the zero normal stress condition of the shell element, two modifications are required in the solution algorithm employed for the concrete layers: (1) modification of the combined concrete material matrix $[D_{cz}]$, and (2) modification of the concrete pseudostress vector $\{\sigma^o_{cz}\}$. Modification of in-plane steel reinforcement layers is not required because the steel material matrices do not contain out-of-plane (normal or shear) stiffness terms.

Because the total out-of-plane strain ε_z is not directly calculated from the displacement field of the finite element, the assumption that the out-of-plane normal stress is negligible, i.e., $\sigma_{cz_z} = 0$, results in

$$\varepsilon_z = \frac{1}{D_{cz_{33}}}(\sigma^o_{cz_z} - D_{cz_{31}} \cdot \varepsilon_x - D_{cz_{32}} \cdot \varepsilon_y - D_{cz_{34}} \cdot \gamma_{xy} - D_{cz_{35}} \cdot \gamma_{xz} - D_{cz_{36}} \cdot \gamma_{yz}) \tag{19}$$

To enforce the zero out-of-plane stress condition in the material matrix, ε_z in Eq. (16) is replaced by the right-hand side of Eq. (19). Simplification yields the removal of the column and row entries pertaining to the local z-direction, i.e., row 3 and column 3 of the 6×6 matrix, according to

$$D^*_{cz_{ij}} = D_{cz_{ij}} - \frac{D_{cz_{i3}} D_{cz_{3j}}}{D_{cz_{33}}} \tag{20}$$

The modified material matrix $[D^*_{cz}]$ is 5×5 in dimension and no longer dependent on ε_z or σ_{cz_z}. The pseudostress vector requires similar modification

$$\sigma^{o*}_{cz_i} = \sigma^o_{cz_i} - \frac{D_{cz_{i3}} \sigma^o_{cz_i}}{D_{cz_{33}}} \tag{21}$$

The resulting equilibrium equation is independent of the out-of-plane normal stress and strain and is of the form required for implementation within the shell finite-element formulation

$$\begin{Bmatrix} \sigma_{cz_x} \\ \sigma_{cz_y} \\ \tau_{cz_{xy}} \\ \tau_{cz_{xz}} \\ \tau_{cz_{yz}} \end{Bmatrix} = [D^*_{cz}]_{5\times5} \begin{Bmatrix} \varepsilon_x \\ \varepsilon_y \\ \gamma_{xy} \\ \gamma_{xz} \\ \gamma_{yz} \end{Bmatrix} - \begin{Bmatrix} \sigma^{o*}_{cz_x} \\ \sigma^{o*}_{cz_y} \\ \tau^{o*}_{cz_{xy}} \\ \tau^{o*}_{cz_{xz}} \\ \tau^{o*}_{cz_{yz}} \end{Bmatrix} \tag{22}$$

Solution Algorithm

The adopted solution method uses a total load secant stiffness approach. The stiffness matrix $[K]$ is evaluated using the secant material matrices developed previously. The full loads acting on the structure are assembled in the total nodal load vector $\{F\}$, and the nodal displacement vector $\{\delta\}$ represents the total displacements under $\{F\}$. Expressed generally

$$\{\delta\} = [K]^{-1}\{F\} \tag{23}$$

The global stiffness matrix is developed through assembly of the elemental stiffness matrices $[k_e]$. Similarly, elemental load vectors $\{f_e\}$ comprise the global nodal load vector

$$[K] \leftarrow \sum_e [k_e] \tag{24}$$

$$\{F\} \leftarrow \sum_e \{f_e\} \tag{25}$$

where the elemental stiffness matrices are defined as

$$[k_e] = \int_{\text{vol}} [B]^T [D][B] dv \tag{26}$$

To accommodate the through-thickness integration procedure employed, matrix $[D]$ in Eq. (26) represents either a concrete or steel layer material matrix, and matrix $[B]$ represents the strain-displacement relations for a given point within the element. Pseudostresses resulting from strain offsets are accommodated by way of pseudoload vectors denoted as $\{f^o_e\}$. Pseudoload vectors are calculated from the following relation:

$$\{f^o_e\} = \int_{\text{vol}} [B]\{\sigma^o\} dv \tag{27}$$

where $\{\sigma^o\}$ represents the concrete and steel layer pseudo-stress vectors defined previously. Inclusion of the structure pseudoload vector $\{F^o\}$ results in the following revised equilibrium expression:

$$\{\delta\} = [K]^{-1}(\{F\} + \{F^o\}) \tag{28}$$

Owing to the nonlinear nature of the problem, the unknown nodal displacement values $\{\delta\}$ are required for the development of the global stiffness matrix $[K]$. As such, an iterative solution procedure is adopted. For a given load step or increment, the iterative procedure is repeated until the solution has converged within a predefined tolerance or a predefined maximum number of iterations has been performed. Convergence is evaluated using the change in the nodal displacement values computed from one iteration to the next.

Out-of-Plane Shear

From a preliminary assessment of the analytical procedure developed, it was found that the constant out-of-plane shear strain distribution employed through the depth of the Mindlin shell element (Fig. 5) typically resulted in overestimation of out-of-plane shear strength, particularly in the case of shear-critical elements. For simple beam-type specimens under combined flexure and out-of-plane shear, the analytical procedure computed artificially large shear stresses within the uncracked compressive regions of the beams and, in some cases, allowed the full shear demand to be carried in less than 10% of the section height. Moreover, the largest strength overestimations were found to occur in members containing no out-of-plane shear reinforcement, which was of primary concern given that RC shell structures often contain little or no out-of-plane reinforcement.

Prior studies employing sectional analyses have demonstrated successes in estimating the out-of-plane shear strength of RC members using a broad range of methods. The simpler approaches that were involved assumed out-of-plane shear strain or shear flow distributions (Vecchio and Collins 1988) and some of the more complex methods utilized rigorous dual-section analyses (Vecchio and Collins 1988) or explicit numerical techniques (Bentz 2000). Although the complex methods have generally demonstrated superior accuracy over simpler approximate solutions, they are computationally expensive and are not well-suited for finite elements that typically rely on deformation assumptions in their formulation, e.g., Mindlin theory.

A vast amount of research has been performed in an effort to improve on the constant out-of-plane shear strain distribution commonly employed for layered finite elements. The research can generally be divided into two categories: (1) development of higher order shear deformation theories (HSDTs), which serve as a replacement of first-order theory, and (2) the development of modification methods that are used in conjunction with first-order theory. In the case of higher order theories, nonuniform out-of-plane shear strains arise from the use of higher order equations describing the element displacement field. The primary benefit of this approach is that nonuniform through-thickness shear strains are calculated directly from nodal displacements without subsequent calculation. However, HSDT approaches often require the solution of additional degrees of freedom and these methods tend to deviate from the well-accepted plane section assumption. Some have proposed simple modifications to first-order shear deformation theory which incorporate nonuniform out-of-plane shear strain distributions but still consider plane section behavior (Tanov and Tabiei 2000; Han et al. 2008). However, the use of such methods has been primarily limited to the analysis of thin laminar-composite elements, and it has been suggested that the methods involving partial modification of the element displacement field may result in appreciable error for other types of structural elements (Han et al. 2008).

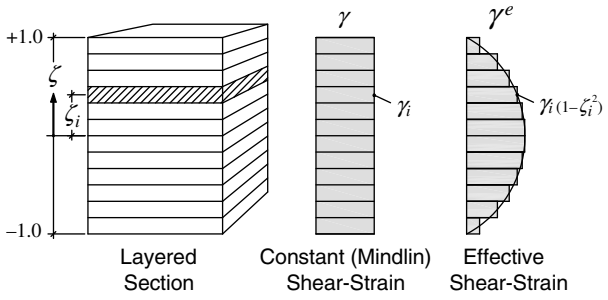

Fig. 5. Out-of-plane shear strain distribution

In most modified first-order formulations, alteration of the strain-displacement relations form the basis of the imposed modifications; however, the procedure developed in this study introduces an effective out-of-plane shear strain concept that is used to alter the out-of-plane shear response without modification of the element displacement field. This approach is developed specifically for nonlinear analyses and is suitable for shell elements possessing either partial or fully populated stiffness matrices with coupled in-plane and out-of-plane relations. The presented formulation is developed on the basis of an effective parabolic out-of-plane shear strain distribution through the depth of the element; however, the equations can be recast to accommodate other shear strain approximations. Prior analytical studies employing the parabolic shear strain approximation through the depths of RC beams under combined axial forces, shear forces, and bending moments have been shown to reasonably estimate solutions obtained using more rigorous computation methods (Vecchio and Collins 1988).

Recall from Eq. (1) that the local strain state for concrete layer i (Fig. 5), which was developed from the element displacement field, is expressed as

$$\{\varepsilon\}_i = \langle\, \varepsilon_{x,i} \quad \varepsilon_{y,i} \quad \gamma_{xy,i} \quad \gamma_{xz,i} \quad \gamma_{yz,i} \,\rangle \tag{29}$$

To introduce the effective strain concept, the out-of-plane shear strain terms in Eq. (29) are assumed to be composed of two contributing parts: effective strains and ineffective strains. Effective shear strains are used to define concrete material stiffness and may be composed of net strains, elastic offsets, plastic offsets, and slip-strain offsets [refer to Eq. (5)]. The ineffective shear strains are independent of material response and treated as additional elastic offsets that are computed in accordance with some assumed out-of-plane shear strain distribution. In the case of the parabolic out-of-plane shear strain distribution considered in this study, the effective and ineffective shear strains are defined using

$$\gamma_{xz,i} = \gamma^e_{xz,i} + \gamma^{ie}_{xz,i} = \gamma_{xz,i}(1 - \zeta_i^2) + \gamma_{xz,i}(\zeta_i^2) \tag{30a}$$

$$\gamma_{yz,i} = \gamma^e_{yz,i} + \gamma^{ie}_{yz,i} = \gamma_{yz,i}(1 - \zeta_i^2) + \gamma_{yz,i}(\zeta_i^2) \tag{30b}$$

where the γ^e terms represent the effective out-of-plane shear strains; the γ^{ie} terms represent the ineffective shear strains; and ζ_i is used to define the location of concrete layer i within the depth of the shell element (refer to Fig. 5).

The local concrete material matrix pertaining to layer i, $[D^*_{cz}]$, is computed on the basis of the DSFM using the modified strain vector $\{\varepsilon^e\}_i$, which is composed of the original in-plane strain terms and effective out-of-plane shear strain terms

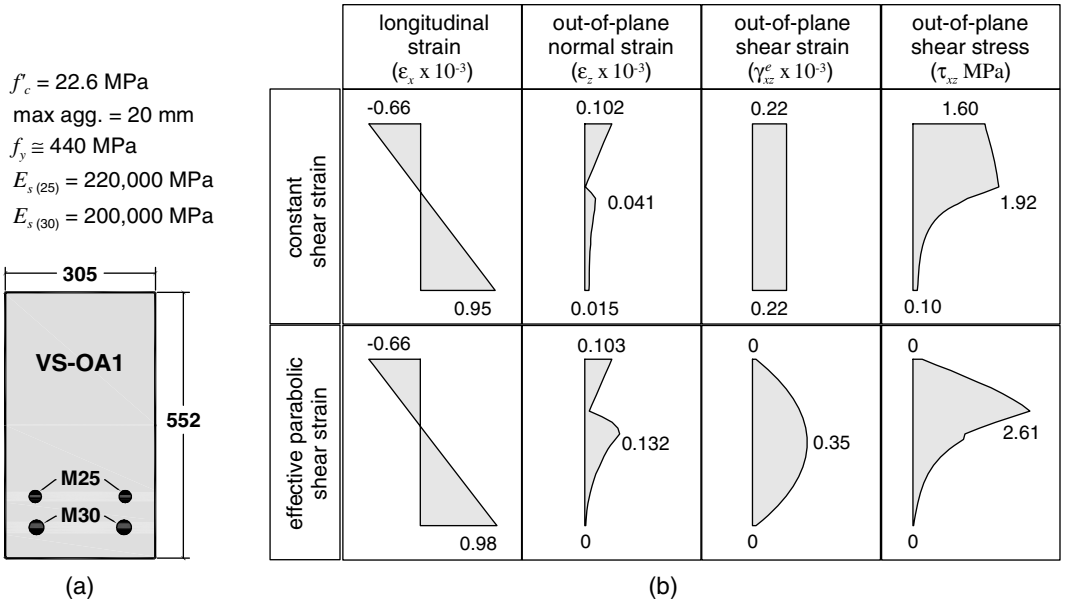

Fig. 6. Sectional analysis of RC Beam VS-OA1: (a) beam cross section; (b) computed sectional response; $M_x = 160$ kN · m; $V_{xz} = 155$ kN

$$\{\varepsilon^e\}_i = \langle \varepsilon_{x,i} \quad \varepsilon_{y,i} \quad \gamma_{xy,i} \quad \gamma^e_{xz,i} \quad \gamma^e_{yz,i} \rangle \tag{31}$$

Eq. (32) presents the resulting equilibrium relation. The introduction of the pseudostress vector $\{\sigma^{ie}\}_i$ is used to modify the relation such that local stresses are calculated using the original local strain vector presented in Eq. (29)

$$\{\sigma_{cz}\}_i = [D^*_{cz}]_i\{\varepsilon^e\}_i - \{\sigma^{o*}_{cz}\}_i \tag{32a}$$

$$\{\sigma_{cz}\}_i + \{\sigma^{o*}_{cz}\}_i = [D^*_{cz}]_i\{\varepsilon^e\}_i = ([D^*_{cz}]_i\{\varepsilon\}_i - \{\sigma^{ie}\}_i) \tag{32b}$$

where the pseudostress $\{\sigma^{ie}\}_i$ is calculated as

$$\{\sigma^{ie}\}_i = [D^*_{cz}]_i\langle 0 \quad 0 \quad 0 \quad \gamma^{ie}_{xz,i} \quad \gamma^{ie}_{yz,i} \rangle \tag{33}$$

The pseudostress vector representing the ineffective shear strain contribution is considered in the solution algorithm by way of nodal pseudoloads using the methodology described previously.

This out-of-plane modification method ensures that equilibrium is always preserved, with sectional forces counterbalancing forces computed from the global equilibrium. The material stiffness matrix remains a function of the original strain-displacement relations permitting simple finite-element implementation and insignificant computational cost.

To illustrate the effect of the out-of-plane shear strain modification procedure developed, consider the computed sectional responses for RC Beam VS-OA1 presented in Fig. 6. The simply supported RC beam formed part of an experimental investigation performed by Vecchio and Shim (2004) and contained no out-of-plane shear reinforcement. The beam had a span of 3,660 mm, an overall depth of 552 mm, and was monotonically loaded to failure by way of increasing displacements applied at the beam's midspan. A half-span finite-element model of the symmetric beam was created using eight shell elements, which were subdivided into 30 equal thickness concrete layers and two longitudinal reinforcement layers (Fig. 7). Fig. 6(b) shows that the out-of-plane sectional behavior of the beam, both normal and shear, is significantly influenced by the out-of-plane shear modification procedure introduced. Under identical loading conditions, the effective parabolic shear strain assumption provides reduced shear stresses in the near-surface compressive layers of the section, increased shear strains at the middepth of the section, reduced shear strains at the extreme fibers of the section, and increased out-of-plane normal strains throughout the cracked layers of the section. The computed load-deflection behaviors for Beam VS-OA1 resulting from the constant and effective parabolic shear strain profiles are compared alongside the experimental response in Fig. 8. Illustrated by the abrupt and severe reductions in the computed load resistance

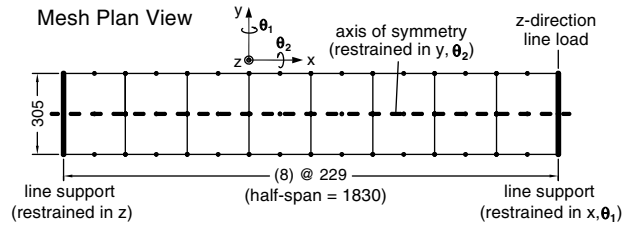

Fig. 7. Finite-element mesh for Beam VS-OA1

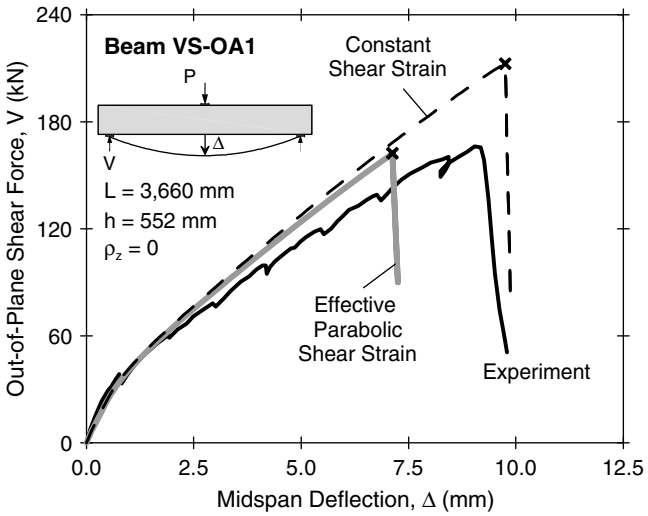

Fig. 8. Computed load-deflection response; Beam VS-OA1

immediately following the maximum estimated capacities, both analyses were successful in capturing the brittle diagonal tension failure that governed the ultimate behavior of the shear-critical RC beam. However, the results developed using the effective out-of-plane shear strain procedure provided a strength estimate that is approximately 25% lower than that computed using the constant shear strain assumption, and, in this case, the use of the parabolic strain profile estimated the capacity of the beam within approximately 5% of the experimentally reported value.

Verification

To assess the adequacy of the developed analysis procedure, the results obtained from analyses of the RC slab and shell elements are presented. The relevance of the experimental data selected for verification is discussed, and information regarding finite-element model development is provided. In applying the formulations of the DSFM, the supporting material models listed in Table 1 were used for all of the reported analyses.

Jaeger and Marti Slabs

In 2005, an international prediction competition involving the analysis of large-scale RC slabs subjected to out-of-plane shear was organized (Jaeger and Marti 2009b). The four slabs comprising the competition, denoted as Slabs A–D, were designed to study the effect of several influential variables: the overall slab height h, which was 200 or 500 mm, the orientation of the in-plane reinforcement φ, which was aligned with the slab edges or skewed by an angle of 45°, and the out-of-plane reinforcement ratio ρ_z. The slabs constructed with skewed reinforcement configurations serve as particularly appealing candidates for analytical verification because the skewed reinforcement configurations were reported to produce three-dimensional stress states in the concrete. Each slab was constructed with a region that contained no out-of-plane shear reinforcement, and each slab was tested twice under one-way simply supported loading conditions. Test 1 was performed on slab segments containing no out-of-plane reinforcement, and Test 2 was performed on slab segments with shear reinforcement [Fig. 9(a)]. The cylindrical compressive strengths of the concretes comprising the slabs ranged from approximately 52 to 59 MPa, and the in-plane and out-of-plane reinforcement consisted of headed deformed steel bars with yield strengths ranging from approximately 480 to 550 MPa. Table 2 provides a summary of the reinforcement configurations and geometric properties of the slabs.

A total of 36 layered shell elements were used to model each slab. Taking advantage of symmetry, half-width finite-element models representing the interior span and only one of the exterior cantilever spans were created. The shell elements were subdivided into 35 concrete layers. A clear cover of 20 mm was specified for 200-mm-deep slabs (Slabs A and B), and a clear cover of 50 mm was applied for 500-mm-deep slabs (Slabs C and D). The in-plane reinforcement was modeled using four additional steel layers for slabs with skewed reinforcement and three additional layers for the slabs with nonskewed reinforcement. When present, out-of-plane reinforcement was smeared throughout the noncover concrete layers. Fig. 9(b) presents the finite-element mesh created for Slabs C and D. The analyses were performed in a displacement controlled manner, with incremental displacements applied to the cantilever load location considered in the testing program. Displacement increments of 1 mm were used for Slabs A and B, and increments of 2 mm were used for Slabs C and D.

Fig. 10 plots the computed moment-displacement responses from each of the eight tests alongside the experimental results.

Table 1. Material Models Considered

Model description	Reference
Concrete compression curve	Hoshikuma et al. (1997)
Compression softening	Vecchio (2000)
Tension stiffening	Bentz (2005)
Concrete confinement	Kupfer et al. (1969), and Richart et al. (1928)
Concrete dilatation	Kupfer et al. (1969)
Crack slip distortions	Walraven and Reinhardt (1981)
Crack spacing	Comité EURO-International du Béton (1990)
Reinforced hysteresis	Seckin (1981)

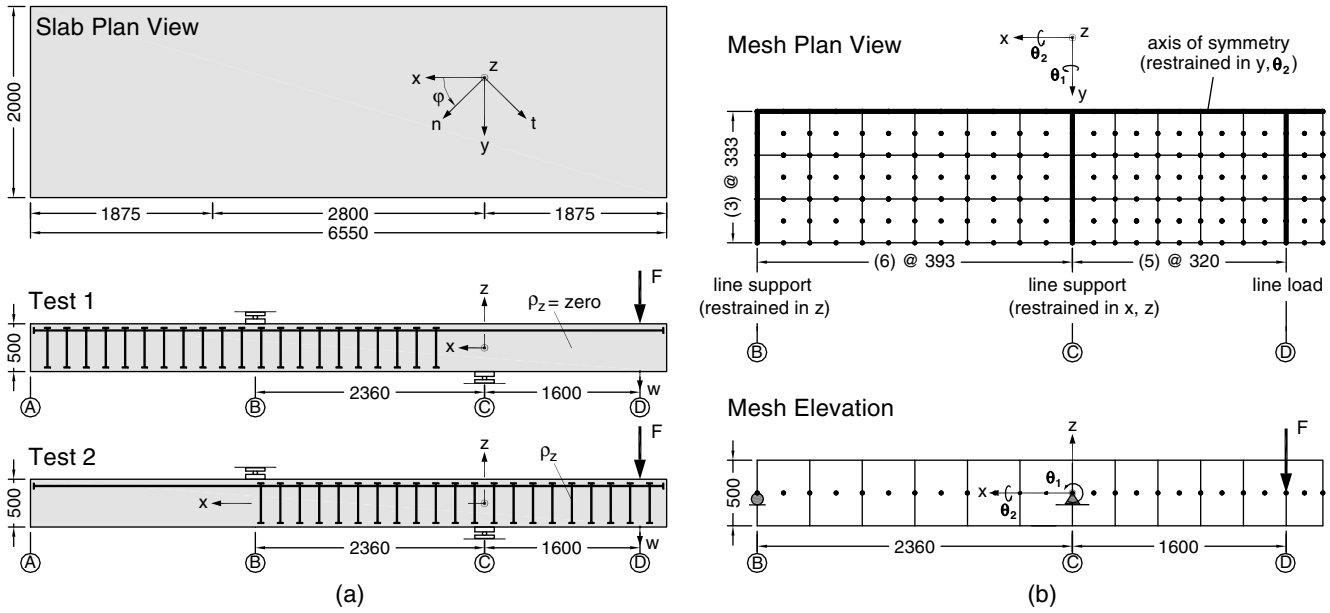

Fig. 9. Specimen configuration and finite-element modeling; Jaeger and Marti Slabs C and D: (a) test setup; (b) finite-element mesh

Table 2. Jaeger and Marti Slab Details

Slab property	Slab A	Slab B	Slab C	Slab D
h (mm)	200	200	500	500
d_{eff} (mm)	156	162	390	405
L (mm)	2,620	2,620	6,550	6,550
b (mm)	800	800	2,000	2,000
φ (degrees)	45	0	45	0
ρ_n (%)[a]	1.812	1.745	1.812	1.745
ρ_t (%)[a]	1.812	0.873	1.812	0.873
$\rho_{z,\text{Test}-1}$ (%)	0	0	0	0
$\rho_{z,\text{Test}-2}$ (%)	0.611	0.309	0.611	0.308

[a]Fig. 9(a) for governing n, t-coordinate system.

It is shown that the analyses of the slab segments without shear reinforcement (Test 1) accurately captured the brittle shear failure modes observed in the laboratory and provided strength estimates within approximately 10% of the experimental values. Analyses of the slab segments containing out-of-plane shear reinforcement (Test 2) provided reasonable estimates of the ultimate capacities but generally underestimated ductility. The reported flexural crushing failure modes and development of lateral (y-direction in Fig. 9) concrete crushing observed on the tension side surfaces of the slabs containing skewed reinforcement were also captured in the analyses of the shear strengthened slab segments. Lastly, because slab height served as one of the primary variables considered in the test series, it is worth noting that similar levels of accuracy were obtained for both thin ($h = 200$ mm) and thick ($h = 500$ mm) slabs. For example, in the case of Slabs A and C, which were nominally identical with the exception of slab geometry, the experimental shear stress capacities, taken as $V/(b \cdot d)$, obtained for the non-shear reinforced slab segments (Test 1) were 1.35 and 1.08 MPa, respectively. The computed shear stress capacities for Slabs A and C were estimated to be 1.22 and 0.99 MPa, respectively. It is evident that reduced shear stress capacity attributed to the increased slab depth was captured in the analyses.

Jaeger and Marti concluded that the behaviors of the slabs forming the competition were very difficult to capture analytically, and predictions developed using finite-element analysis techniques were generally found to produce poor slab response estimates. On the basis of the criteria used to judge the competition entries (Jaeger and Marti 2009a), the finite-element analysis results presented in this paper would have fared best. Albeit not blind, the analyses were performed using simple finite-element meshing techniques without refinement. No fine tuning of analysis parameters or material models was performed, and the material models employed required basic user input consisting of parameters that are easily defined.

Adebar and Collins Shells

In the late 1980s, Adebar and Collins carried out an experimental program (Adebar and Collins 1991) to investigate the interaction behavior of RC elements subjected to combined in-plane and out-of-plane shear forces. Shell-type RC elements that were approximately 1,600 × 1,600 mm, with thicknesses of either 310 or 410 mm, were tested using a large-scale machine capable of applying coexisting membrane forces, bending moments, and out-of-plane shear forces (Kirschner and Collins 1986). Each shell element was reinforced with two sets of orthogonal in-plane reinforcement grids, with equal reinforcement ratios provided in the orthogonal directions. Five of the shell elements that were similar in terms of geometry, reinforcement configuration, and material properties but were subjected to different membrane to out-of-plane shear stress ratios have been analyzed using the proposed procedure. All of the

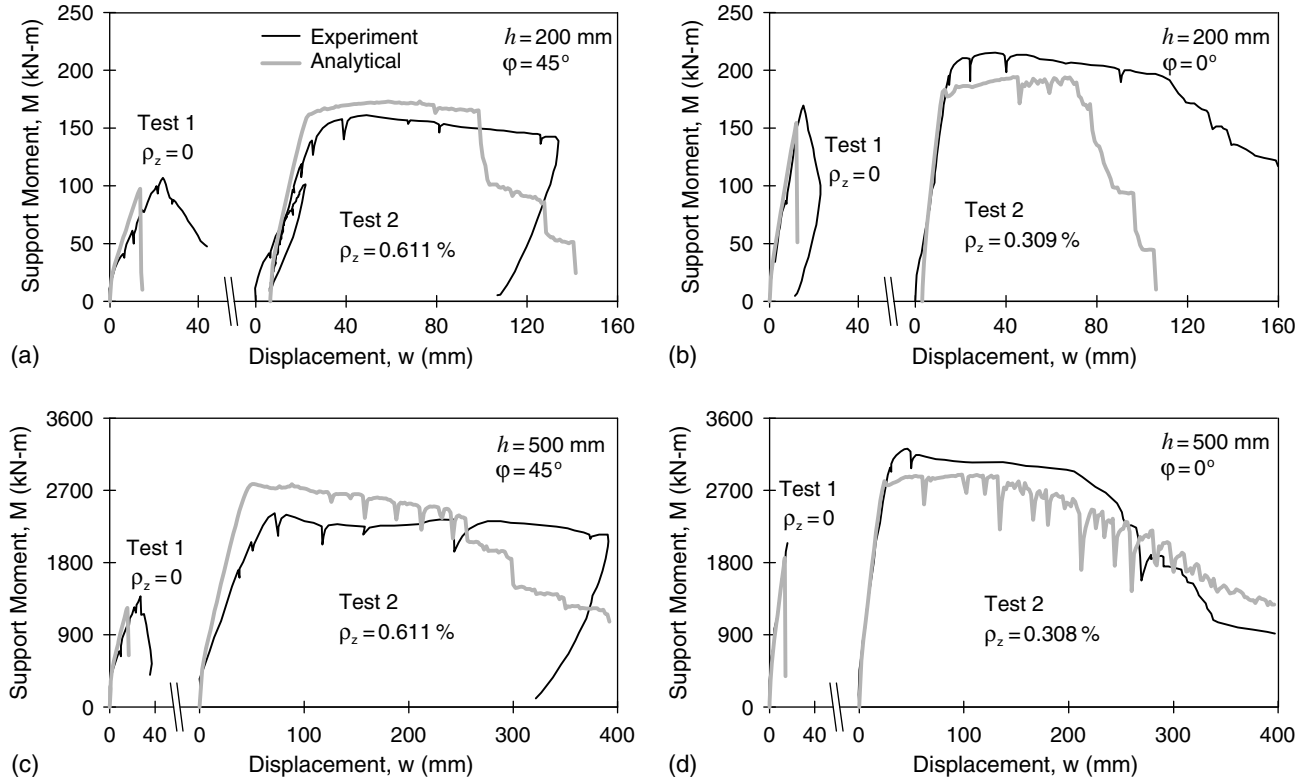

Fig. 10. Computed moment-displacement responses; Jaeger and Marti slabs: (a) Slab A; (b) Slab B; (c) Slab C; (d) Slab D

shell elements considered in the following discussion were 310 mm thick, contained in-plane reinforcement skewed at an angle of 45° from the specimen edges, and were lightly reinforced in the out-of-plane direction ($\rho_z = 0.08\%$). Table 3 presents a summary of the details and loading conditions considered for these shell elements.

The RC shell elements were subjected to out-of-plane shear forces and bending moments about a single axis. Taking advantage of symmetry, a finite-element mesh consisting of 18 layered shell elements representing half of the planar surface of the specimens was developed and used for all of the analyses performed (Fig. 11). The layered shell finite elements were subdivided into 30 concrete layers, and an additional four layers were used to represent the in-plane reinforcing bars. A clear cover of 20 mm was considered for the top and bottom surfaces of the elements, and out-of-plane shear reinforcement was smeared throughout the core concrete layers. Loads in the form of normal membrane forces and out-of-plane shear forces were applied along the perimeter of the finite-element mesh and produced conditions of uniform in-plane shear stress and constant out-of-plane shear force, respectively. Fig. 11 illustrates the variation of the bending moment and the constant out-of-plane shear force attributed to the restraint and loading conditions provided. Loads were applied in fixed proportions using increments of approximately 1% of the reported experimental load capacities. Table 4 summarizes the analytical results and compares them with the experimental values. In addition, Fig. 12 plots the analytical in-plane to out-of-plane shear interaction behavior alongside the experimental results. The presented analytical response was computed using the average nominal properties listed in the figure.

Fig. 12 shows that the general trend developed from the finite-element analyses agrees well with the strength interaction response observed in the experimental program. In agreement with reported results, the in-plane compression developed perpendicular to the bending plane, i.e., in a direction that would contribute to the closing of the cracks developed under the out-of-plane loads, led to increased shear resistances and failure modes controlled by concrete crushing (refer to the right-hand side of Fig. 12). Additive in-plane tension led to reduced element capacities and tension-controlled shear failures that were estimated to occur shortly after yielding of the out-of-plane shear reinforcement. With the exception of SP8, which was subjected to pure in-plane shear stress conditions, all of the shell elements experienced out-of-plane shear failures before yielding the in-plane reinforcement. The governing failure modes estimated from the finite-element analyses were in agreement with those observed. For the five shell elements

Table 3. Adebar and Collins Shell Details

	Shell				
Element details	SP3	SP4	SP7	SP8	SP9
Loading[a]	0:1	4:1	−4:1	1:0	−8:1
f'_c (MPa)	49.8	52.4	54.1	52.9	49.6
Aggregate (mm)[b]	10	10	20	20	20
ρ_s (%)[c]	3.58	3.58	3.75	3.75	3.75
f_y (MPa)	480	480	536	536	536

[a]Ratio of in-plane shear stress to out-of-plane shear stress.
[b]Maximum nominal aggregate size.
[c]Total reinforcement ratio in each planar orthogonal direction.

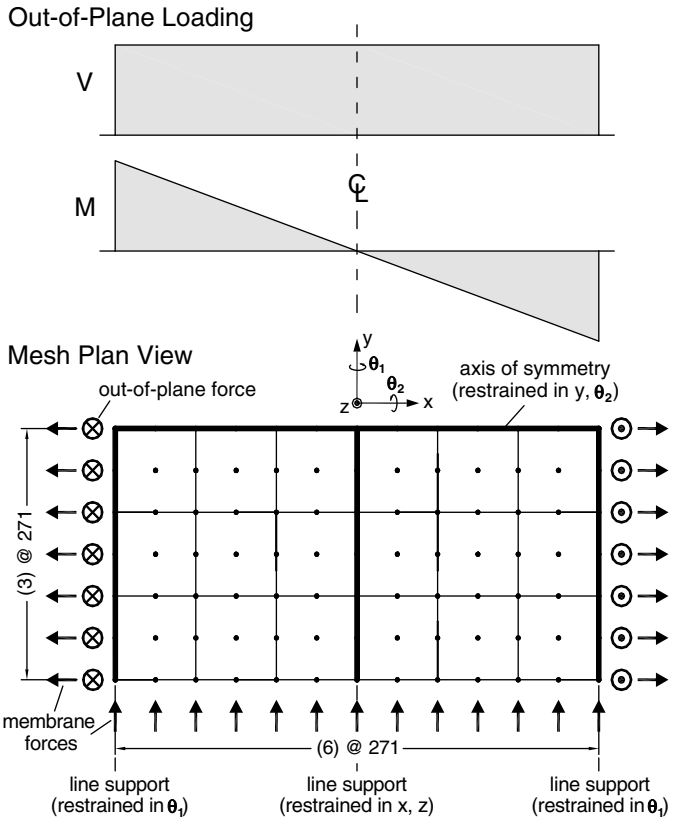

Fig. 11. Loading configuration and finite-element mesh; Adebar and Collins shells

Table 4. Results for Adebar and Collins Shells

	Experiment (E_{XP})		Analysis (A_N)		
Shell	$v_{u,\mathrm{OOP}}$ (MPa)[a]	$v_{u,\mathrm{IP}}$ (MPa)	$v_{u,\mathrm{OOP}}$ (MPa)[a]	$v_{u,\mathrm{IP}}$ (MPa)	A_N/E_{XP}
SP3	1.75	0	1.54	0	0.88
SP4	2.15	8.60	2.44	9.76	1.13
SP7	1.60	−6.40	1.41	−5.64	0.88
SP8	0	±16.80	0	±18.60	1.11
SP9	1.22	−9.76	1.23	−9.84	1.01
Mean	—	—	—	—	1.00
SD (%)	—	—	—	—	10.8

Note: IP = in plane; OOP = out of plane.
[a]$V/(b \cdot h)$.

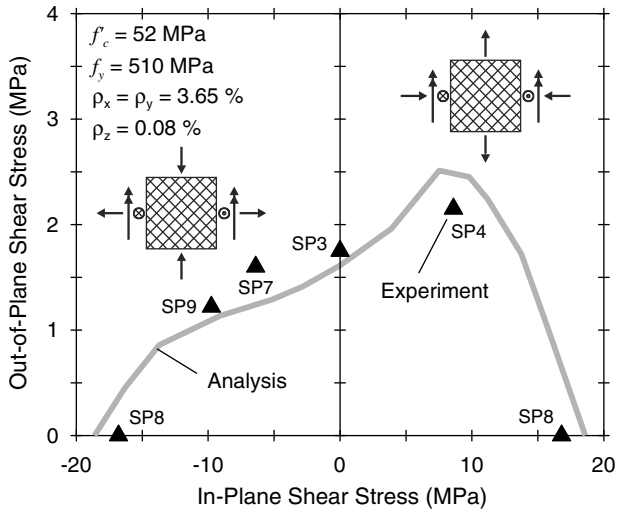

Fig. 12. Computed shear stress interaction response; Adebar and Collins shells

considered, the mean analytical-to-experimental capacity ratio was determined to be a value of 1.00, with a standard deviation of approximately 11%. For RC elements such as these, which contain very light through-thickness shear reinforcement and are subjected to appreciable out-of-plane shear loads, this level of precision is deemed adequate.

Conclusions

In this study, a procedure for nonlinear finite-element analysis of RC slabs and shells is presented. An effective out-of-plane shear strain concept is introduced to modify the through-thickness response of the layered shell finite elements employed. The adequacy of the resulting nonlinear analysis program was verified using experimental data pertaining to RC slabs and shells subjected to combined in-plane and out-of-plane loading scenarios, several of which were governed by out-of-plane shear failures. The work presented in this study supports the following conclusions:

1. The nonlinear finite-element analysis procedure that was developed in accordance with the formulations of the disturbed stress field model serves as a viable approach for the analysis of RC slabs and shell structures under three-dimensional loading conditions.
2. The introduction of an effective out-of-plane shear strain procedure was shown to significantly alter the through-thickness response of the Mindlin layered finite elements and provided improved shear strength estimates for the shear-critical RC elements. Furthermore, the modification method is simple to implement, requires insignificant additional computation cost, and can be employed in cases in which in-plane and out-of-plane material behavior is coupled, i.e., the material matrix is fully populated.
3. The analysis procedure was shown to provide accurate estimates of strength, damage development, and governing modes of failure for RC elements that were governed by brittle shear-critical out-of-plane failure modes.
4. The behaviors of RC elements controlled by flexural crushing were captured well in terms of capacity, damage, and governing failure mode; however, analytical estimates tended to underestimate the ductility levels that were observed experimentally.

Acknowledgments

Financial support provided by the Natural Sciences and Engineering Research Council of Canada (NSERC) and by the industry sponsor Morrison Hershfield Ltd. is gratefully acknowledged.

References

Adebar, P. E. (1989). "Shear design of concrete offshore structures." Ph.D. dissertation, Univ. of Toronto, Toronto.

Adebar, P. E., and Collins, M. P. (1991). "Shear design of concrete offshore structures." *ACI Struct. J.*, 91(3), 324–335.

Bentz, E. C. (2000). "Sectional analysis of reinforced concrete members." Ph.D. dissertation, Univ. of Toronto, Toronto.

Bentz, E. C. (2005). "Explaining the riddle of tension stiffening models for shear panel experiments." *J. Struct. Eng.*, 10.1061/(ASCE)0733-9445(2005)131:9(1422), 1422–1425.

Collins, M. P., and Mitchell, D. (1997). *Prestressed concrete structures*, Response Publications, Toronto/Montreal, Canada.

Comité EURO-International du Béton. (1990). "Model code for concrete structures." *CEB-FIP MC90*.

Cook, R. D., Malkus, D. S., and Plesha, M. E. (1989). *Concepts and applications of finite element analysis*, 3rd Ed., Wiley.

Figueiras, J. A., and Owen, D. R. J. (1984). "Analysis of elasto-plastic and geometrically nonlinear anisotropic plates and shells." *Finite element software for plates and shells*, E. Hinton and D. R. J. Owen, eds., Pineridge, Swansea, U.K.

Han, S. C., Tabiei, A., and Park, W. T. (2008). "Geometrically nonlinear analysis of laminated composite thin shells using a modified first-order shear deformable element-based Lagrangian shell element." *Compos. Struct.*, 82(3), 465–474.

Hand, F. R., Pecknold, D. A., and Schnobrich, W. C. (1973). "Nonlinear analysis of RC plates and shells." *J. Struct. Div.*, 99(ST7), 1491–1505.

Hoshikuma, J., Kawashima, K., Nagaya, K., and Taylor, A. W. (1997). "Stress-strain model for confined reinforced concrete in bridge piers." *J. Struct. Eng.*, 10.1061/(ASCE)0733-9445(1997)123:5(624), 624–633.

Jaeger, T., and Marti, P. (2009a). "Reinforced concrete slab shear prediction competition: Entries and discussion." *ACI Struct. J.*, 106(3), 309–318.

Jaeger, T., and Marti, P. (2009b). "Reinforced concrete slab shear prediction competition: Experiments." *ACI Struct. J.*, 106(3), 300–308.

Kirschner, U., and Collins, M. P. (1986). "Investigating the behaviour of reinforced concrete shell elements." *Publication No. 86-9*, Dept. of Civil Engineering, Univ. of Toronto, Toronto.

Kupfer, H., Hilsdorf, H. K., and Rusch, H. (1969). "Behavior of concrete under biaxial stress." *ACI J.*, 87(2), 656–666.

Lin, C., and Scordelis, A. C. (1975). "Nonlinear analysis of RC shells of general form." *J. Struct. Div.*, 101(ST3), 523–538.

Maekawa, K., Pimanmas, A., and Okamura, H. (2003). *Nonlinear mechanics of reinforced concrete*, Spon, New York, 721.

Mindlin, R. D. (1951). "Influence of rotary inertia and shear on flexural motions of isotropic, elastic plates." *J. Appl. Mech.*, 18(1), 31–38.

Owen, D. R. J., and Figueiras, J. A. (1984). "Ultimate load analysis of reinforced concrete plates and shells." *Finite element software for plates and shells*, E. Hinton and D. R. J. Owen, eds., Pineridge, Swansea, U.K.

Polak, M. A., and Vecchio, F. J. (1993). "Nonlinear analysis of reinforced-concrete shells." *J. Struct. Eng.*, 10.1061/(ASCE)0733-9445(1993)119:12(3439), 3439–3462.

Richart, F. E., Brandtzaeg, A., and Brown, R. L. (1928). "A study of the failure of concrete under combined compressive stresses." *Bulletin 185*, Univ. of Illinois, Engineering Experimental Station, Urbana, IL.

Schnobrich, W. C. (1977). "Behavior of reinforced concrete structures predicted by the finite element method." *Comput. Struct.*, 7(3), 365–376.

Seckin, M. (1981). "Hysteretic behaviour of cast-in-place exterior beam-column-slab subassemblies." Ph.D. dissertation, Univ. of Toronto, Toronto.

Song, H., Shim, S., Byun, K., and Maekawa, K. (2002). "Failure analysis of reinforced concrete shell structures using layered shell element with pressure node." *J. Struct. Eng.*, 10.1061/(ASCE)0733-9445(2002)128:5(655), 655–664.

Tanov, R., and Tabiei, A. (2000). "A simple correction to the first-order shear deformation shell finite element formulations." *Finite Elem. Anal. Des.*, 35(2), 189–197.

Vecchio, F. J. (2000). "Disturbed stress field model for reinforced concrete: Formulation." *J. Struct. Eng.*, 10.1061/(ASCE)0733-9445(2000)126:9(1070), 1070–1077.

Vecchio, F. J., and Collins, M. P. (1986). "The modified compression-field theory for reinforced concrete elements subjected to shear." *ACI J. Proc.*, 83(2), 219–231.

Vecchio, F. J., and Collins, M. P. (1988). "Predicting the response of reinforced concrete beams subjected to shear using the modified compression field theory." *ACI Struct. J.*, 85(3), 258–268.

Vecchio, F. J., and Shim, W. (2004). "Experimental and analytical re-examination of classic concrete beam tests." *J. Struct. Eng.*, 10.1061/(ASCE)0733-9445(2004)130:3(460), 460–469.

Walraven, J. C., and Reinhardt, H. W. (1981). "Theory and experiments on the mechanical behaviour of cracks in plain and reinforced concrete subjected to shear loading." *Concr. Mech. Part A*, 26(4), 65.